

Novel GaAs surface phases via direct control of chemical potentialC. X. Zheng,¹ J. Tersoff,^{2,*} W. X. Tang,^{3,†} A. Morreau,⁴ and D. E. Jesson^{4,‡}¹*Department of Civil Engineering, Monash University, Victoria 3800, Australia*²*IBM T. J. Watson Research Center, Yorktown Heights, New York 10598, USA*³*School of Physics, Monash University, Victoria 3800, Australia*⁴*School of Physics and Astronomy, Cardiff University, Cardiff CF24 3AA, United Kingdom*

(Received 6 December 2015; revised manuscript received 23 April 2016; published 24 May 2016)

Using *in situ* surface electron microscopy, we show that the surface chemical potential of GaAs (001), and hence the surface phase, can be systematically controlled by varying temperature with liquid Ga droplets present as Ga reservoirs. With decreasing temperature, the surface approaches equilibrium with liquid Ga. This provides access to a regime where we find phases ultrarich in Ga, extending the range of surface phases available in this technologically important system. The same behavior is expected to occur for similar binary or multicomponent semiconductors such as InGaAs.

DOI: [10.1103/PhysRevB.93.195314](https://doi.org/10.1103/PhysRevB.93.195314)**I. INTRODUCTION**

GaAs surfaces are of great scientific and technological importance, and have been intensively studied over the years (see, e.g., Refs. [1–13]). Much of this work has focused on the (001) surface, which is used in most electronic applications. This surface exhibits a variety of structures having different surface composition, ranging from the As-rich $c(4\times 4)$ and (2×4) phases through to the Ga-rich $c(8\times 2)$, (6×6) , and (4×6) phases. Particular surface phases of differing structure and composition are used in the growth of optoelectronic materials, InGaAs quantum devices, and dilute magnetic semiconductors for spintronics by molecular beam epitaxy. In addition, surface composition is known to be critical for the incorporation of elements such as Bi to adjust the lattice constant and band gap [14]. It is also important in the fabrication of low-density GaAs quantum dots via droplet epitaxy for potential applications as quantum light sources [15]. This has led to significant efforts to understand and control the stability of surface phases as a function of experimental conditions, as well as to seek ways of accessing different structures to influence growth mechanisms for potential device applications [1–15].

At fixed temperature, the stable structure (the one with the lowest Gibbs free surface energy) depends on the values of the Ga and As chemical potentials. Control of surface chemical potential is therefore paramount in order to stabilize surface phases. It is well appreciated that transitions between As-rich surface phases can be induced by varying the As flux and/or the substrate temperature [1–3]. The control of Ga-rich phases is more challenging, but careful work has shown how deposition of Ga can be used to stabilize very Ga-rich surfaces (see, e.g., Refs. [1,11]). Ultimately, one would like a method to map the equilibrium phase diagram in this Ga-rich regime by incrementally adjusting the surface chemical potential.

Here we describe an approach to controlling the chemical potential of surfaces by slowly varying the substrate temperature with liquid droplets present as Ga reservoirs. In the case of GaAs (001), this allows the surface phases to approach equilibrium with Ga liquid at low temperature, enabling us to attain an extreme Ga-rich limit. This regime is explored by *in situ* surface electron microscopy. We find novel surface phases which are stabilized by the high Ga chemical potential, thereby extending the experimentally accessible GaAs (001) phase diagram in this technologically important system.

II. EXPERIMENT

Experiments were performed in an ultrahigh-vacuum (UHV), low-energy electron microscope (LEEM) specially designed for III-V epitaxy [16]. Temperatures T were measured using an infrared pyrometer, including a correction due to the T dependence of the surface emissivity [17] and calibrated to the congruent evaporation temperature T_c of 625 °C [18,19]. We degassed a (001)-oriented undoped GaAs sample at 300 °C for 24 h. This was followed by high-temperature flashing up to 600 °C and annealing at 580 °C for 2 h to remove the surface oxide. Ga droplets of radius $\sim 2\ \mu\text{m}$ were prepared by annealing above T_c at 650 °C, and the droplets were allowed to run across the surface [20,21], creating smooth planar (001) regions which we utilize for our imaging experiments [22]. A mirror electron microscope (MEM) image of a set of droplets and smooth trails is shown in Fig. 1(a). Droplets appear in the MEM as a uniform dark disk somewhat larger than the actual droplet, surrounded by a concentric bright ring [23]. The droplet density on the sample was $\sim 7\times 10^{-3}\ \mu\text{m}^{-2}$. The specific (001) region used to image surface phases using LEEM is displayed in Fig. 1(b) and is within 10 μm of the accompanying droplet.

The sample was then carefully annealed at a series of decreasing temperatures, from 580 °C down to 300 °C. At temperatures where phase transformations were observed, the relevant temperature range was scanned in reduced increments to identify the transition temperature. To ensure that the observed phase distributions had fully stabilized, each annealing temperature was held constant for 60 min. The phase transformations observed were all found to be fully reversible.

*tersoff@us.ibm.com

†Present address: College of Materials Science and Engineering, Chongqing University, Chongqing 400044, People's Republic of China.

‡jessonde@cardiff.ac.uk

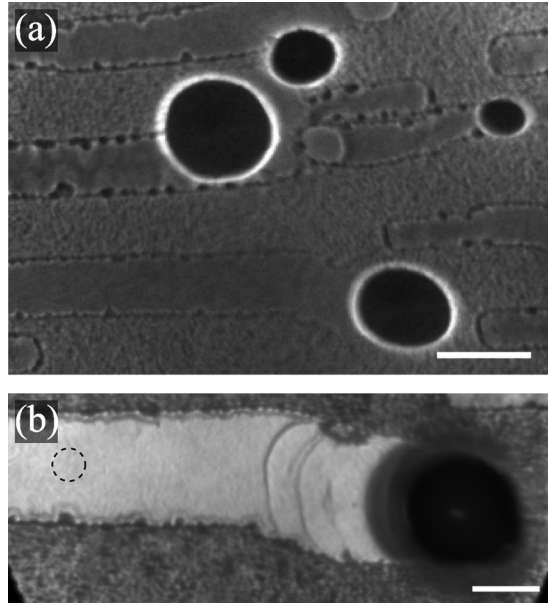


FIG. 1. (a) MEM image of a set of planar (001) trail regions produced by the motion of Ga droplets. The primary electron energy was 20 keV and this was offset with respect to surface potential by -0.3 eV. (b) LEEM image of the planar (001) region used for the phase transformation studies. The dashed circle indicates the position of the illumination aperture used to collect the μ LEED diffraction data in Fig. 2. The electron energy is 2.4 eV. The scale markers in (a) and (b) are 5 and 2 μm , respectively.

Figure 2(a) contains a LEEM image of a planar (001) region with accompanying micro-low-energy electron diffraction (μ LEED) pattern. The dashed circle indicates the position of the illumination aperture used to collect the μ LEED diffraction data and is within 10 μm of the accompanying droplet. A schematic diffraction pattern is also shown, where large circles indicate the positions of (1×1) spots. In Fig. 2(a) the μ LEED pattern reveals a pure $c(8 \times 2)$ phase which was found to exist down to $\sim 540^\circ\text{C}$, as indicated on the left-hand side of Fig. 3.

Upon decreasing the annealing temperature further, $c(8 \times 2)$ is found to coexist over a small temperature range with a phase of (6×6) periodicity which we term $(6 \times 6)D$ [Fig. 2(b)]. This phase is clearly disordered along $[\bar{1}10]$ as indicated by the μ LEED pattern. Upon decreasing T below 540°C , the dominant mixture is a combination of $c(8 \times 2)$ and (4×6) . This is surprising since it is believed the ultrarich Ga (4×6) phase can only be obtained following deposition of Ga [1,11,15]. Eventually, below 530°C , an unforeseen $c(2 \times 12)$ phase appears as shown in Fig. 2(c), coexisting with (4×6) . Note that a small amount of residual $c(8 \times 2)$ phase is always stabilized at surface steps throughout the experiments. Extremely weak, disordered $(n \times 6)$ μ LEED streaks are also observed along $[110]$ directions in the range $400\text{--}500^\circ\text{C}$.

To establish that Ga droplets are responsible for the unexpected phases, we completely removed the droplets from the surface by annealing below T_c at 570°C . Flat trail regions were again imaged by LEEM and the $c(8 \times 2)$ phase was observed at the sample annealing temperature $T = 580^\circ\text{C}$. This is the most Ga-rich phase observed during annealing without droplets [1,7]. As T is decreased, a transition to the

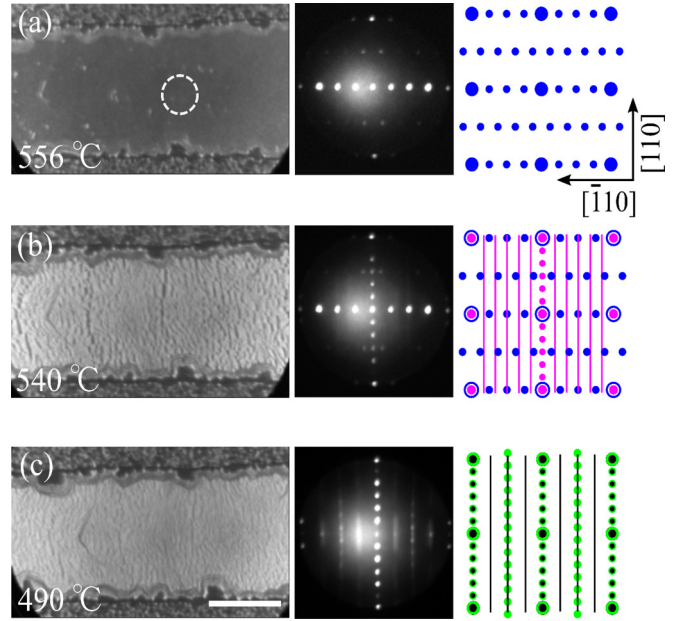


FIG. 2. LEEM images and accompanying μ LEED diffraction patterns obtained from a GaAs(001) planar region with liquid Ga droplets present on the surface. The dashed circle in (a) indicates the position of the illumination aperture used to collect the μ LEED diffraction data. The scale marker in (c) is 2 μm across. Schematic diffraction patterns are also shown, where large circles indicate the positions of (1×1) spots. In (a) the pattern indicates a pure $c(8 \times 2)$ phase. (b) $c(8 \times 2)$ coexists with $(6 \times 6)D$ (superimposed red spots and lines). $(6 \times 6)D$ is disordered along $[\bar{1}10]$ and differs from the (6×6) phase observed without droplets (see text). (c) Phase coexistence between (4×6) (black) and a high-periodicity $c(2 \times 12)$ phase (green). Each phase distribution was carefully stabilized by annealing for 60 min. The electron energy was 2.4 eV for LEEM imaging and 10.3 eV for μ LEED diffraction.

less Ga-rich (6×6) phase is observed at around 525°C , which is separated by a region of phase coexistence. This is in good agreement with the observations of others, who observe these phases at high and low temperatures, respectively, during

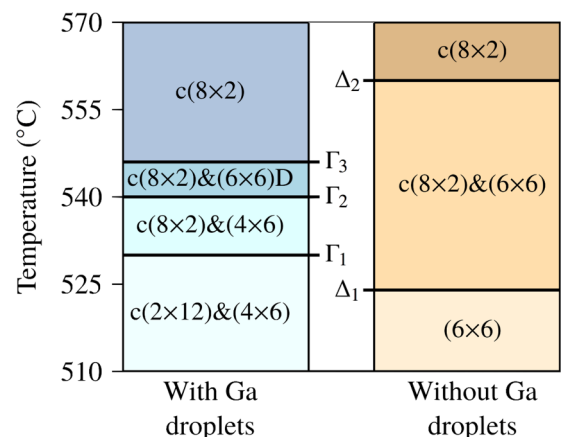


FIG. 3. Phase diagram with and without droplets deduced from LEEM imaging and μ LEED as a function of temperature (see Fig. 2). Phase transformations with and without droplets occur at boundaries Γ_1 , Γ_2 , Γ_3 and Δ_1 , Δ_2 , respectively.

annealing [1,5,9,11]. We note that the relative intensities of the (6×6) LEED spots without droplets are very different from the (6×6)*D* phase observed with droplets present. We therefore expect that (6×6)*D* may have basically the same structure as (4×6), but with a different periodicity to accommodate slightly different amounts of excess Ga, while the normal (6×6) phase could be a very different structure [5,13].

III. THEORY

We can explain the very different phase diagrams observed in the presence and absence of droplets by considering the competing pathways for Ga atoms. In the absence of droplets, Ga is lost by evaporation, but decomposition of GaAs provides a source of Ga that increases rapidly with temperature. The net result is that the surface becomes more Ga rich at higher temperatures. When droplets are present, they provide an additional source of surface Ga. At high temperature, evaporation and decomposition may still dominate, because the entire surface contributes. However, with decreasing temperature, the surface approaches equilibrium with the droplets because of the lower energy barriers associated with Ga adatom detachment from the droplets compared to evaporation or GaAs decomposition. As a result, while the bare surface becomes less Ga rich with decreasing *T*, the surface with droplets present becomes more Ga rich.

To illustrate this behavior concretely, we propose a simple model describing the Ga balance at a GaAs surface at temperature *T*, with or without droplets present. The surface is assumed to be in equilibrium with the crystal so that $\mu_{\text{Ga}} + \mu_{\text{As}} = \mu_{\text{GaAs}}$ where μ_{Ga} and μ_{As} are the respective Ga and As surface chemical potentials, and μ_{GaAs} is the chemical potential (per two-atom unit) of the bulk crystal. Let us first consider the case of a droplet-free surface. Assuming a standard transition rate model for Ga and As evaporation, the respective evaporation rates per unit area are

$$F_{\text{Ga}} = r_{\text{Ga}} \exp\left(\frac{\mu_{\text{Ga}} - E_{\text{Ga}}}{kT}\right) \quad (1)$$

and

$$F_{\text{As}} = N r_{\text{As}} \exp\left(\frac{N\mu_{\text{GaAs}} - N\mu_{\text{Ga}} - E_{\text{As},N}}{kT}\right). \quad (2)$$

This assumes that As evaporates as an *N*-mer (most likely a dimer). E_{Ga} and $E_{\text{As},N}$ are the respective transition state energies for Ga adatom and As *N*-mer evaporation, with associated rate constants r_{Ga} and r_{As} including the transition state entropy or degeneracy, e.g., the number of sites for evaporation per unit area. In Eq. (2), F_{As} is defined per atom independent of *N*, while r_{As} refers to *N*-mer desorption events.

In the absence of droplets, μ_{Ga} is determined by congruent evaporation from the surface. We denote this as μ_{Ga}^b , where *b* refers to the bare, droplet-free surface. During congruent evaporation, μ_{Ga}^b attains a steady-state value such that Ga and As evaporate at equal rates ($F_{\text{Ga}} = F_{\text{As}}$). Evaporation of As has a larger activation barrier than Ga evaporation, and so as *T* increases, the increased As evaporation causes Ga to accumulate on the surface, which, in turn, increases μ_{Ga} until $F_{\text{Ga}} = F_{\text{As}}$ is restored. However, if μ_{Ga} rises above the liquidus value $\mu_{\text{Ga}}^l(T_c)$ at temperature T_c , then droplets can form, which

defines the upper limit for congruent evaporation. As long as there are no droplets present, from Eqs. (1) and (2) we can obtain the surface chemical potential μ_{Ga}^b (see the Appendix),

$$\mu_{\text{Ga}}^b = \mu_{\text{Ga}}^l(T_c) + c_k(T - T_c), \quad (3)$$

where c_k is a constant related to the kinetics of evaporation.

Now consider the surface in the presence of Ga droplets, as in Fig. 1. Our LEEM experiments show that the phase transformations occur uniformly over distances greater than the average droplet separation, so we assume attachment/detachment limited kinetics for Ga moving between surface and droplet. Then the Ga chemical potential on the surface with droplets present, μ_{Ga}^d , is to a good approximation spatially uniform. The droplets act as a source (or sink) for surface Ga adatoms at a rate

$$F_d = r_d \exp\left(\frac{-E_d}{kT}\right) \left[\exp\left(\frac{\mu_{\text{Ga}}^l}{kT}\right) - \exp\left(\frac{\mu_{\text{Ga}}^d}{kT}\right) \right], \quad (4)$$

where μ_{Ga}^l is the chemical potential of the liquid droplet, and $r_d = s_d k_d$, where s_d is the perimeter length of the droplets per unit area of the surface, and k_d and E_d are the respective rate constant and activation energy for attachment at the droplet perimeter. We assume that the droplet is nearly in equilibrium with the GaAs substrate at liquidus composition.

To obtain μ_{Ga}^d we assume that the surface is in a quasisteady state so that $F_{\text{As}} + F_d = F_{\text{Ga}}$, i.e., surface Ga resulting from As evaporation and net detachment from the droplet is equal to the Ga lost by evaporation; and we neglect the reduction in surface area by droplet coverage. Combining Eqs. (1), (2), and (4) for *N* = 2 with this steady-state condition then yields

$$\exp\left(\frac{3\mu_{\text{Ga}}^d}{kT}\right) - \frac{r_d \exp\left(\frac{2\mu_{\text{Ga}}^d + \mu_{\text{Ga}}^l - E_d}{kT}\right)}{r_{\text{Ga}} \exp\left(\frac{-E_{\text{Ga}}}{kT}\right) + r_d \exp\left(\frac{-E_d}{kT}\right)} - \frac{2r_{\text{As}} \exp\left(\frac{2\mu_{\text{GaAs}} - E_{\text{As},2}}{kT}\right)}{r_{\text{Ga}} \exp\left(\frac{-E_{\text{Ga}}}{kT}\right) + r_d \exp\left(\frac{-E_d}{kT}\right)} = 0. \quad (5)$$

This is a cubic equation in $\exp(\mu_{\text{Ga}}^d/kT)$, and μ_{Ga}^d is the real solution (see the Appendix). Our model, consisting of Eq. (5) for μ_{Ga}^d and Eq. (3) for μ_{Ga}^b , describes the temperature dependence with and without droplets in terms of three material parameters c_k , r_{Ga}/r_d , and $(E_d - E_{\text{Ga}})$ (see the Appendix).

The chemical potentials μ_{Ga}^d , μ_{Ga}^b , and μ_{Ga}^l are plotted in Fig. 4 for illustrative values of the parameters, since the actual values are not known. Ideally we would like to use the chemical potential as a direct guide to how Ga rich the surface will be. However, in fact the chemical potentials all decrease with increasing temperature due to the vibrational contributions to the free energy. To make the plot a better

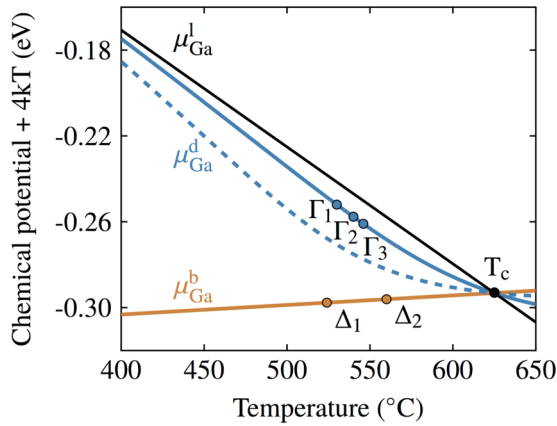


FIG. 4. Model for the variation of Ga chemical potential with temperature. μ_{Ga}^d and μ_{Ga}^b are the respective Ga surface chemical potentials with and without droplets present. The droplet chemical potential μ_{Ga}^l is well approximated by that of liquid Ga, evaluated from the thermodynamic data contained in Ref. [28]. μ_{Ga}^b and μ_{Ga}^d (solid line) are calculated from Eqs. (3) and (5), respectively, using illustrative values $c_k = -37 \text{ eV K}^{-1}$, $r_{\text{Ga}}/r_d = 30$, and $(E_d - E_{\text{Ga}}) = -0.35 \text{ eV}$. The temperatures of the actual phase transformations in Fig. 3 are indicated on the μ_{Ga}^b and μ_{Ga}^d curves. The dashed curve represents μ_{Ga}^d for a factor-of-4 decrease in droplet perimeter per unit area. A value of $4kT$ has been added to the vertical chemical potential axis to make the plots more readable.

indicator of Ga richness when comparing surfaces at different T , we subtract out a rough estimate ($-4kT$) of the surface vibrational free energy, plotting $\mu + 4kT$ [24]. The curve for the bare surface chemical potential μ_{Ga}^b monotonically rises with increasing temperature, reflecting a more Ga-rich surface. (This behavior extends above T_c , since droplets do not nucleate at a detectable rate when μ_{Ga}^b is only slightly above μ_{Ga}^l , due to a large barrier for Ga droplet nucleation.) This variation of μ_{Ga}^b produces the transition between $c(8 \times 2)$ and (6×6) via a transition zone involving phase coexistence (Fig. 3). Regions of coexistence separating distinct phases appear to be a regular feature of this system [1,2,5,9,25], resulting from long-range electrostatic and elastic interactions between surface domains [26,27].

When droplets are present on the surface, they act as reservoirs of Ga at liquidus chemical potential μ_{Ga}^l . For the temperature range of interest, the droplet contains less than 0.3% As and so μ_{Ga}^l is well approximated by that of pure liquid Ga, which can be evaluated from thermodynamic data [28]. μ_{Ga}^l is plotted in Fig. 4 and decreases quite rapidly with increasing T due to the large liquid entropy compared with the crystal solid.

The surface chemical potential in the presence of droplets, μ_{Ga}^d , as evaluated from Eq. (5) for an illustrative set of parameters, is plotted in Fig. 4, and can be seen to lie in between the limits of the liquidus μ_{Ga}^l and the evaporation-dominated bare-surface μ_{Ga}^b . At T_c , the surface chemical potential must be equal to the Ga liquidus value whether or not droplets are present. Insofar as the kinetics are dominated by evaporation at this temperature, the slopes of μ_{Ga}^d and μ_{Ga}^b start to approach each other close to T_c .

Below 575°C , evaporation from the GaAs (001) surface is much reduced [29]. The attachment barrier at the droplet (E_d) is expected to be much smaller than the energy barriers controlling evaporation (E_{Ga} , $E_{\text{As},N}$), so with decreasing T , F_d plays an increasingly important role compared with F_{Ga} and F_{As} in determining μ_{Ga}^d . At sufficiently low T , we expect that F_d becomes so dominant that the condition for mass balance reduces to $F_d \approx 0$, i.e., the surface approaches equilibrium with the droplet and $\mu_{\text{Ga}}^d \approx \mu_{\text{Ga}}^l$.

For a given T , increasing the number or size of droplets increases the droplet perimeter length per unit area, and hence the parameter r_d . As can be seen from Fig. 4, this shifts the crossover to the droplet-dominated regime to higher temperatures.

IV. DISCUSSION

We can now explain the experimentally observed sequence of phases as a function of temperature as illustrated in Fig. 4. Without droplets, the surface is most Ga rich at high T with the chemical potential approximately equal to $\mu_{\text{Ga}}^l(T_c)$. However, with droplets present, the surface is most Ga rich at low T . Close to T_c , $\mu_{\text{Ga}}^d \approx \mu_{\text{Ga}}^b$, so the observed surface reconstruction $c(8 \times 2)$ is identical in both cases. However, as T decreases further, the behavior of the Ga surface chemical potential in the presence of droplets is very different. Since the activation energy for droplet attachment/detachment is lower than the activation barrier for Ga evaporation, μ_{Ga}^d rises above $\mu_{\text{Ga}}^l(T_c)$, accessing a different regime of high Ga chemical potential. This leads to the appearance of novel phase mixtures; first $c(8 \times 2)$ with $(6 \times 6)D$ and then $c(8 \times 2)$ with (4×6) . The (4×6) phase has been previously observed following deposition of Ga [1,11,15], but is stabilized here by the droplet modified surface chemical potential, which significantly exceeds $\mu_{\text{Ga}}^l(T_c)$.

There has been considerable interest in seeking the most extreme Ga-rich phase of GaAs (001) [1,4,5,11]. (4×6) is presently regarded as the most Ga-rich phase [1,11]. However, our capability to control chemical potential via T in the presence of a droplet reservoir and to establish equilibrium within an ultrarich Ga phase space has produced an unexpected $c(2 \times 12)$ phase which is seen to coexist with (4×6) below 530°C . The $12 \times$ LEED features represent the highest reconstruction periodicity observed along a symmetry axis to date [5]. Since $c(2 \times 12)$ occurs under extreme Ga-rich surface conditions induced by Ga droplets, it is also clearly a strong candidate for the most Ga-rich phase found to date.

Most analyses of GaAs surface phases have been based on density functional theory (DFT) calculations of the enthalpy at $T = 0$. In that case, the Ga-rich limit is defined by equilibrium with solid Ga (see, for example, Ref. [11]). However, at the much higher T of experiments, the Ga-rich limit is defined by equilibrium with liquid Ga. This corresponds to a much less Ga-rich surface than in $T = 0$ calculations, because the liquid has substantial extra entropy, making it a stronger sink for Ga (lower chemical potential relative to GaAs). While the surface chemical potential is close to that of liquid Ga at high temperature near T_c , the most Ga-rich surfaces can only be reached via equilibrium with liquid Ga at far lower temperatures, where the contribution from the excess entropy of the liquid is reduced.

V. CONCLUSION

In summary, we have developed a method of controlling the chemical potential of GaAs surfaces, under UHV conditions, using liquid droplets as a reservoir for Ga. By varying the temperature, it is possible to carefully control and extend the range of the chemical potential so that the surface approaches equilibrium with the droplet. This stabilizes a high-periodicity $c(2 \times 12)$ phase in a regime ultrarich in Ga. Such phases may have applications in quantum structure fabrication [3,15] and enhanced elemental incorporation [14]. We also anticipate the use of droplets to access previously unobtainable regimes and to create different surface structures will see wide applicability in other technologically important systems such as GaN and InGaAs.

ACKNOWLEDGMENT

D.E.J. acknowledges support from a Marie Curie International Incoming Fellowship. We are grateful to Zhenyu Zhou and Shane Kennedy for important discussions.

APPENDIX

1. Free energies in terms of enthalpy and entropy at a fixed temperature

We can write the Gibbs free energy at temperature T in terms of the enthalpy H and entropy S as

$$G(T) = H(T) - TS(T). \quad (\text{A1})$$

If we expand around some temperature T_0 in our experimental range of interest, we obtain

$$G(T) \approx G(T_0) + (T - T_0)G'(T_0), \quad (\text{A2})$$

which, from (A1), can be written

$$\begin{aligned} G(T) &\approx G(T_0) + (T - T_0)[H'(T_0) - S(T_0) - T_0S'(T_0)] \\ &= G(T_0) + (T - T_0)[H'(T_0) - T_0S'(T_0)] \\ &\quad - (T - T_0)S(T_0). \end{aligned} \quad (\text{A3})$$

However, at constant pressure the heat capacity $C_P = dH/dT = TdS/dT$, and we can write

$$G(T) \approx G(T_0) - (T - T_0)S(T_0), \quad (\text{A4})$$

which, from (A1), gives

$$G(T) \approx H(T_0) - TS(T_0). \quad (\text{A5})$$

We subsequently assume that the temperature dependence of all free energies and chemical potentials can be approximated in this form.

2. Derivation of bare surface chemical potential μ_{Ga}^b in the absence of droplets

All symbols are defined in the main text. Assuming a standard transition rate model for Ga and As evaporation, the respective evaporation rates per unit area are

$$F_{\text{Ga}} = r_{\text{Ga}} \exp\left(\frac{\mu_{\text{Ga}} - E_{\text{Ga}}}{kT}\right) \quad (\text{A6})$$

and

$$F_{\text{As}} = Nr_{\text{As}} \exp\left(\frac{N\mu_{\text{GaAs}} - N\mu_{\text{Ga}} - E_{\text{As},N}}{kT}\right), \quad (\text{A7})$$

with $\mu_{\text{Ga}} + \mu_{\text{As}} = \mu_{\text{GaAs}}$. Congruent evaporation implies $F_{\text{As}} = F_{\text{Ga}}$,

$$\begin{aligned} r_{\text{Ga}} \exp\left(\frac{\mu_{\text{Ga}} - E_{\text{Ga}}}{kT}\right) \\ = Nr_{\text{As}} \exp\left(\frac{N\mu_{\text{GaAs}} - N\mu_{\text{Ga}} - E_{\text{As},N}}{kT}\right). \end{aligned} \quad (\text{A8})$$

Hence,

$$(N+1)\mu_{\text{Ga}} = kT \ln\left(\frac{Nr_{\text{As}}}{r_{\text{Ga}}}\right) + N\mu_{\text{GaAs}} + E_{\text{Ga}} - E_{\text{As},N}. \quad (\text{A9})$$

Now μ_{GaAs} is equivalent to the crystal free energy per atom pair given by $G_{\text{GaAs}} = H_{\text{GaAs}} - TS_{\text{GaAs}}$, where H_{GaAs} and S_{GaAs} are the respective enthalpy and entropy, so we can write (A9) as

$$\begin{aligned} (N+1)\mu_{\text{Ga}} &= kT \left[\ln\left(\frac{Nr_{\text{As}}}{r_{\text{Ga}}}\right) - N\frac{S_{\text{GaAs}}}{k} \right] \\ &\quad + NH_{\text{GaAs}} + E_{\text{Ga}} - E_{\text{As},N}. \end{aligned} \quad (\text{A10})$$

At $T = T_c$ we have $\mu_{\text{Ga}} = \mu_{\text{Ga}}^l(T_c)$ which, from (A10), gives

$$\begin{aligned} (N+1)\mu_{\text{Ga}} &= (N+1)\mu_{\text{Ga}}^l(T_c) + k(T - T_c) \\ &\quad \times \left[\ln\left(\frac{Nr_{\text{As}}}{r_{\text{Ga}}}\right) - N\frac{S_{\text{GaAs}}}{k} \right]. \end{aligned} \quad (\text{A11})$$

Therefore,

$$\mu_{\text{Ga}} = \mu_{\text{Ga}}^b = \mu_{\text{Ga}}^l(T_c) + c_k(T - T_c), \quad (\text{A12})$$

where

$$c_k = \frac{k}{(N+1)} \left[\ln\left(\frac{Nr_{\text{As}}}{r_{\text{Ga}}}\right) - N\frac{S_{\text{GaAs}}}{k} \right]. \quad (\text{A13})$$

3. Independent parameters governing μ_{Ga}^b

We assume that S_{GaAs} and the transition state entropies contained in r_{Ga} and r_{As} are defined at $T_0 = 525^\circ\text{C}$. $S_{\text{GaAs}} = 55.9 \text{ J mol}^{-1} \text{ K}^{-1}$ is obtained from fitting $G_{\text{GaAs}} = H_{\text{GaAs}} - TS_{\text{GaAs}}$ to thermodynamic data [28], which leaves $r_{\text{As}}/r_{\text{Ga}}$, or equivalently the slope c_k , as the only free parameter.

4. Derivation of surface chemical potential μ_{Ga}^d in the presence of droplets

The droplets act as a source (or sink) for surface Ga adatoms at a rate

$$F_d = r_d \exp\left(\frac{-E_d}{kT}\right) \left[\exp\left(\frac{\mu_{\text{Ga}}^l}{kT}\right) - \exp\left(\frac{\mu_{\text{Ga}}^d}{kT}\right) \right]. \quad (\text{A14})$$

The condition for the quasisteady state is $F_{As} + F_d = F_{Ga}$, so that from (A6), (A7), and (A14) we have

$$0 = \left[r_{Ga} \exp\left(\frac{-E_{Ga}}{kT}\right) + r_d \exp\left(\frac{-E_d}{kT}\right) \right] \exp\left(\frac{(N+1)\mu_{Ga}^d}{kT}\right) - r_d \exp\left(\frac{-E_d}{kT}\right) \exp\left(\frac{\mu_{Ga}^l}{kT}\right) \exp\left(\frac{N\mu_{Ga}^d}{kT}\right) - Nr_{As} \exp\left(\frac{N\mu_{GaAs} - E_{As,2}}{kT}\right). \quad (A15)$$

Substituting $\mu_{GaAs} = H_{GaAs} - TS_{GaAs}$, $\mu_{Ga}^l = H_{Ga}^l - TS_{Ga}^l$, where H_{Ga}^l and S_{Ga}^l are the respective Ga liquid enthalpy and

entropy, then with $N = 2$ we can rewrite (A15) as

$$x^3 - b(T)x^2 - c(T) = 0. \quad (A16)$$

The chemical potential is obtained from the real solution $x = \exp(\mu_{Ga}^d/kT)$ with

$$b(T) = \frac{\exp\left(\frac{H_{Ga}^l}{kT}\right) \exp\left(-\frac{S_{Ga}^l}{k}\right)}{\frac{r_{Ga}}{r_d} \exp\left(\frac{E_d - E_{Ga}}{kT}\right) + 1},$$

$$c(T) = \frac{2 \frac{r_{As}}{r_{Ga}} \frac{r_{Ga}}{r_d} \exp\left(\frac{2H_{GaAs} - E_{As,2} + E_d}{kT}\right) \exp\left(-\frac{2S_{GaAs}}{k}\right)}{\frac{r_{Ga}}{r_d} \exp\left(\frac{E_d - E_{Ga}}{kT}\right) + 1}. \quad (A17)$$

5. Independent parameters governing μ_{Ga}^d

$H_d^l = 18.9 \text{ kJ mol}^{-1}$, $S_d^l = 85.8 \text{ J mol}^{-1} \text{ K}^{-1}$, and $S_{GaAs} = 55.9 \text{ J mol}^{-1} \text{ K}^{-1}$ are known from fitting thermodynamic data [28]. This leaves r_{Ga}/r_d and $(E_d - E_{Ga})$ as independent parameters. In addition, we need to know $(2H_{GaAs} - E_{As,2} + E_d)$, which can be expressed in terms of the other unknown parameters by noting that at $T = T_c$ we have $\mu_{Ga}^d = \mu_{Ga}^l(T_c)$, so that from (A16) and (A17) we obtain

$$2H_{GaAs} - E_{As,2} + E_d = kT_c \ln \left[\frac{1}{2 \frac{r_{As}}{r_{Ga}} \frac{r_{Ga}}{r_d}} \left(\frac{r_{Ga}}{r_d} \exp\left(\frac{E_d - E_{Ga}}{kT_c}\right) + 1 \right) \exp\left(\frac{2S_{GaAs}}{k}\right) \left[\exp\left(\frac{3\mu_{Ga}^l(T_c)}{kT_c}\right) - b(T_c) \exp\left(\frac{2\mu_{Ga}^l(T_c)}{kT_c}\right) \right] \right]. \quad (A18)$$

Since c_k is a function of r_{As}/r_{Ga} [(A13)], the three independent parameters for μ_{Ga}^d are c_k , r_{Ga}/r_d , and $(E_d - E_{Ga})$.

-
- [1] A. Ohtake, *Surf. Sci. Rep.* **63**, 295 (2008).
 [2] V. P. LaBella, M. R. Krause, Z. Ding, and P. M. Thibado, *Surf. Sci. Rep.* **60**, 1 (2005).
 [3] B. A. Joyce and D. D. Vvedensky, *Mater. Sci. Eng., R* **46**, 127 (2004).
 [4] Q. Xue, T. Hashizume, J. M. Zhou, T. Sakata, T. Ohno, and T. Sakurai, *Phys. Rev. Lett.* **74**, 3177 (1995).
 [5] J. G. McLean, P. Kruse, and A. C. Kummel, *Surf. Sci.* **424**, 206 (1999).
 [6] S.-H. Lee, W. Moritz, and M. Scheffler, *Phys. Rev. Lett.* **85**, 3890 (2000).
 [7] A. Ohtake, S. Tsukamoto, M. Pristovsek, N. Koguchi, and M. Ozeki, *Phys. Rev. B* **65**, 233311 (2002).
 [8] A. Ohtake, J. Nakamura, S. Tsukamoto, N. Koguchi, and A. Natori, *Phys. Rev. Lett.* **89**, 206102 (2002).
 [9] M. Pristovsek *et al.*, *Phys. Status Solidi B* **240**, 91 (2003).
 [10] E. Penev, P. Kratzer, and M. Scheffler, *Phys. Rev. Lett.* **93**, 146102 (2004).
 [11] A. Ohtake, P. Kocán, K. Seino, W. G. Schmidt, and N. Koguchi, *Phys. Rev. Lett.* **93**, 266101 (2004).
 [12] M. Takahashi and J. Mizuki, *Phys. Rev. Lett.* **96**, 055506 (2006).
 [13] A. Ohtake, *Phys. Rev. B* **75**, 153302 (2007).
 [14] R. B. Lewis, M. Masnadi-Shirazi, and T. Tiedje, *Appl. Phys. Lett.* **101**, 082112 (2012).
 [15] M. Jo, T. Mano, and K. Sakoda, *Cryst. Growth Des.*, **11**, 4647 (2011).
 [16] D. E. Jesson, and W. X. Tang, in *Microscopy: Science, Technology, Applications and Education*, edited by A. Méndez-Vilas and J. Díaz, Microscopy Book Series No. 4 (FORMATEx, Badajoz, Spain, 2010), Vol. 3, p. 1608.
 [17] P. J. Timans, *J. Appl. Phys.* **72**, 660 (1992).
 [18] J. Y. Tsao, *Materials Fundamentals of Molecular Beam Epitaxy* (Academic, San Diego, CA, 1993).
 [19] Z. Y. Zhou, C. X. Zheng, W. X. Tang, D. E. Jesson, and J. Tersoff, *Appl. Phys. Lett.* **97**121912 (2010).
 [20] J. Tersoff, D. E. Jesson, and W. X. Tang, *Science* **324**, 236 (2009).
 [21] E. Hilner, A. A. Zakharov, K. Schulte, P. Kratzer, J. N. Andersen, E. Lundgren, and A. Mikkelsen, *Nano Lett.* **9**2710 (2009).
 [22] C. X. Zheng, W. X. Tang, and D. E. Jesson, *J. Vac. Sci. Technol. A* **34**, 043201 (2016).
 [23] S. M. Kennedy, C. X. Zheng, W. X. Tang, D. M. Paganin, and D. E. Jesson, *Ultramicroscopy* **111**, 356 (2011).
 [24] A. D. van Langeveld and J. W. Niemantsverdriet, *J. Vac. Sci. Technol. A* **5**, 558 (1987).
 [25] L. E. Sears, J. M. Millunchick, and C. Pearson, *J. Vac. Sci. Technol. B* **26**, 1948 (2008); J. E. Bickel, N. A. Modine, C. Pearson, and J. M. Millunchick, *Phys. Rev. B* **77**, 125308 (2008).
 [26] D. Vanderbilt, *Surf. Sci.* **268**, L300 (1992).
 [27] J. B. Hannon, F.-J. Meyer zu Heringdorf, J. Tersoff, and R. M. Tromp, *Phys. Rev. Lett.* **86**, 4871 (2001).
 [28] I. Ansara *et al.*, *CALPHAD* **18**, 177 (1994).
 [29] C. T. Foxon, J. A. Harvey, and B. A. Joyce, *J. Phys. Chem. Solids* **34**, 1693 (1973).